REPRODUCED AT GOV'T EXPENSE # 49

KAPL-P-000181
(K97073)

VELOCITY AND PHASE DISTRIBUTION MEASUREMENTS IN VERTICAL AIR-WATER ANNULAR FLOWS

P. Vassallo

July 1997

NOTICE

This report was prepared as an account of work sponsored by the United States Government. Neither the United States, nor the United States Department of Energy, nor any of their employees, nor any of their contractors, subcontractors, or their employees, makes any warranty, express or implied, or assumes any legal liability or responsibility for the accuracy, completeness or usefulness of any information, apparatus, product or process disclosed, or represents that its use would not infringe privately owned rights.

KAPL ATOMIC POWER LABORATORY SCHENECTADY, NEW YORK 10701

Operated for the U. S. Department of Energy
by KAPL, Inc. a Lockheed Martin company

MASTER

DISTRIBUTION OF THIS DOCUMENT IS UNLIMITED

DISCLAIMER

This report was prepared as an account of work sponsored by an agency of the United States Government. Neither the United States Government nor any agency thereof, nor any of their employees, makes any warranty, express or implied, or assumes any legal liability or responsibility for the accuracy, completeness, or usefulness of any information, apparatus, product, or process disclosed, or represents that its use would not infringe privately owned rights. Reference herein to any specific commercial product, process, or service by trade name, trademark, manufacturer, or otherwise does not necessarily constitute or imply its endorsement, recommendation, or favoring by the United States Government or any agency thereof. The views and opinions of authors expressed herein do not necessarily state or reflect those of the United States Government or any agency thereof.

DISCLAIMER

Portions of this document may be illegible in electronic image products. Images are produced from the best available original document.

REPRODUCED AT GOV'T EXPENSE # 49

Velocity and Phase Distribution Measurements in Vertical Air-Water Annular Flows

Peter Vassallo

Summary

Annular flow topology for three air-water conditions in a vertical duct is investigated through the use of a traversing double-sensor hot-film anemometry probe and differential pressure measurements. Near wall measurements of mean and fluctuating velocities, as well as local void fraction, are taken in the liquid film, with the highest turbulent fluctuations occurring for the flow condition with the largest pressure drop. A modified law-of-the-wall formulation for wall shear is presented which, using near wall values of mean velocity and kinetic energy, agrees reasonably well with the average stress obtained from direct pressure drop measurements. The linear profile using wall coordinates in the logarithmic layer is preserved in annular flow; however, the slope and intercept of the profile differ from the single-phase values for the annular flow condition which has a thicker, more turbulent, liquid film.

1.0 Introduction

As described by Hewitt and Whalley (1989), annular flow in a conduit consists of a high velocity gas core in the center of the conduit and a thin liquid film on the conduit walls. The interaction between gas core and liquid film produces a wavy structure at the gas-liquid interface which, in turn, affects the turbulent structure in the film. The frictional pressure drop, or wall shear, is ultimately related to the turbulent structure in the film. Quantitative near wall turbulence measurements in annular flow are therefore needed to help develop analytical models, and to qualify numerical codes, which are used to predict overall pressure drop.

Several recent studies in annular and bubbly flow have yielded results which are pertinent to the current work. Hewitt, *et al.* (1990) observed the wavy structure at the gas-liquid interface in annular flows and noted that air bubbles were continuously generated and released by the rolling action of the waves. Lorencez, *et al.* (1997) measured the turbulence level in the gas and liquid phases in horizontal stratified flow and found that the turbulence level in the film increased as the interfacial shear increased. In bubbly flow, Velidandla, *et al.* (1996) and Marie, *et al.* (1997) measured near wall velocities and determined that the linear log-law was preserved near the wall, but with different values of the coefficients.

REPRODUCED AT GOVT EXPENSE # 49

2.0 Experimental Description

2.1 Test Section and Related Instrumentation

The air-water flow loop consists of a transparent test section, pump, air-water separator, and several rotameters and pressure gauges for the measurement of air and water flow rates. A schematic of the test section is given in figure 1. The test section, made from cast acrylic components, is about 170 cm long, with a cross-sectional flow area of 6.35 cm x 0.635 cm (D_h=1.15 cm). The test section has eight removable windows on the transverse walls into which instrumentation may be mounted.

Figure 1 shows the locations of the quick-closing valves and the pressure taps. The quick-closing valves were used to obtain the average static void fraction. The pressure taps (0.25 mm diameter) were installed in two of the test section faces in order to measure the frictional pressure drop. The pressure drop was measured using calibrated Rosemont transducers with an estimated total uncertainty of ±4 %, based on the observed scatter in repeated measurements.

2.2 Hot-Film Anemometry (HFA)

A quartz coated TSI double-sensor hot-film probe (model 1244-10AW) was mounted in a traversing mechanism to allow for motion across the narrow test section dimension. The probe was located near the exit of the test section, at an axial position of Z=152.2 cm (Z/D_h=132) and a transverse position of X=3.2 cm. Each of the probe's two active sensors had an active length of 0.178 mm, and a diameter of 0.038 mm; the spacing between sensors was 1 mm.

The HFA probe was equipped with a pin which extended 0.076 mm past the outermost sensor. This pin protected the sensor from damage as the probe was moved close to the far wall. A 6.35 mm diameter bolt was machined flat and screwed into the far wall to serve as a detection point for the probe. When the pin touched the bolt, a circuit was established and defined the first measurement location at a position 0.762 mm from the wall. The probe was then retracted across the test section as measurements were taken. The uncertainty in HFA positioning was estimated to be ±0.025 mm.

Local void fraction, liquid velocity and interfacial velocity were obtained with the HFA probe. For void fraction and liquid velocity, only the upstream sensor in the double wire probe was used; for interfacial velocity, both sensors were used. The overheat ratio (the ratio of operating resistance to the resistance at ambient temperature) was about 1.1. A total of 6.4 sec of data were taken at each point at a sampling rate of 10 KHz. The water temperature was maintained at 32.2°C ±0.2 °C.

To obtain liquid velocity statistics (both mean and fluctuating quantities), the HFA probe was first calibrated in single-phase liquid flow using Laser Doppler Velocimetry to measure velocity. A constant temperature was maintained at the hot-film; for a given operating resistance, the change in voltage corresponded to a change in velocity. During the early phase of this work, a slow downward drift in HFA voltage was observed at a constant liquid flow rate; apparently, due to

REPRODUCED AT GOV'T EXPENSE # 49

small loop contaminants in the deionized water collecting on the probe and changing its heat transfer characteristics. To reduce contamination uncertainties, the probe was run in the high velocity annular flow condition for about 30 minutes, and then quickly calibrated (in a period of about 5 minutes) over a range of liquid velocities, with the last calibration being a repeat of the first to ensure that significant drift was not occurring. The HFA measurements in the annular flow condition were then taken. Finally, the air was turned off, and the calibration measurements were repeated. This approach effectively eliminated any concerns about drift in the HFA probe voltage during data acquisition.

For determination of liquid velocity, the HFA voltage traces acquired in two-phase flow had to be processed to remove the vapor part of the signals. This was accomplished by using a program developed by Lee (1982) which employs both level and slope thresholding. When a vapor interface contacts the probe, the voltage level decreases abruptly. A slope threshold can be established so that when the voltage gradient exceeds the threshold value, the signal is taken as part of the vapor phase. Level thresholding is also employed to improve the accuracy of the method. The level threshold was obtained by visual examination of the voltage traces. The slope threshold was estimated from oscillscope voltage traces and was about twice the value of the maximum slope observed in all liquid flow. The results were not very sensitive to this selection; Table 1 shows calculated values of void fraction and fluctuating velocities for the same voltage trace as a function of slope and level threshold.

The velocity of the passing interfaces in the two-phase mixture was obtained by cross correlating the signals from each of the two HFA sensors using a signal analyzer. This resulted in a most probable time required for the interfaces to travel between the two sensors. The mean interfacial velocity was calculated by dividing the know sensor spacing (1 mm) by this time. The random uncertainty in velocity, based on repeated measurements, is estimated to be ±5 %.

3.0 Results

3.1 Single-Phase Flow

Single-phase liquid measurements of mean and fluctuating velocities were taken across the test section thickness dimension to verify the HFA technique. The results are presented in terms of Y/t, where Y is the position along the narrow duct dimension and t is the duct thickness. The calibration curve used to determine velocity is shown in figure 2a. The points on the curve were taken before and after the two-phase measurements (presented in Section 3.2) and indicate good repeatability.

Figure 2b shows the mean and fluctuating velocity profiles taken with the HFA probe at Re=21,700 along with profiles taken by Laufer (1951) at Re=39,700 in a 12.7 x152.4 cm duct. The mean profiles agree well; the fluctuating profiles also agree well except that the peak intensity at Y/t=0.02 is somewhat lower than Laufer's. This small disagreement may be explained by the fact that, at a given Reynolds number, the near wall turbulent production is highly sensitive to duct size, with the larger duct sizes having higher turbulence intensities (Laufer (1951)). In any case, the current data, showing smooth and reasonable turbulent profiles, provides a measure of confidence in using HFA to obtain liquid velocity statistics.

REPRODUCED AT GOV'T EXPENSE # 49

3.2 Two-Phase Flow

Three annular flow conditions were investigated: Case (1) j_l=1.3m/s, j_g=12.8m/s; Case (2) j_l=0.65m/s, j_g=20.4m/s and Case (3) j_l=0.65m/s, j_g=25.0m/s. These conditions were chosen to cover a broad range of available gas and liquid flow rates while still maintaining a steady (non-chugging) annular flow. The conditions represent quite different flow topologies: Qualitatively, Case 1 consists of a lower overall void fraction, with a thicker and more turbulent liquid film on the wall, while Cases 2 and 3 have a thinner, steadier film structure. According to the flow pattern map of Hewitt and Roberts (1969), Case 1 lies near the border of the annular and churn-turbulent regime while Cases 2 and 3 are more completely annular. Further discussion based on quantitative measurements for each flow condition is given below.

3.2.1 General Flow Topology

In figure 3, measurements of interfacial velocity and void fraction are presented. The void fraction for all test cases increases rather steeply for $Y/t < 0.1$, increases more gradually for $0.1 < Y/t < 0.2$ and is relatively constant for $0.2 < Y/t < 0.5$. These regions may be roughly interpreted as the liquid film, interfacial wave, and droplet core regions. Visually, the average of the local measurements is in good agreement with the cross-section averaged void fraction obtained with the quick-closing valves, as indicated by the flat lines associated with each set of data This provides a measure of confirmation that the HFA processing algorithm is being correctly applied. The random uncertainty in average void fraction (±2 %) was estimated by repeating measurements of the same flow conditions. The bias uncertainty is believed to be small, based on good comparison with the integrated average of the local HFA void fraction measurements.

3.2.2 Near Wall Measurements

In figure 4, near wall measurements of liquid velocity, interfacial velocity, liquid turbulence intensity and void fraction are presented. These measurements were taken over several days, using appropriate single-phase calibration performed before and after each data set. The largest potential errors in the velocity and turbulence measurements are associated with the calibration uncertainty. To assess the magnitude of this uncertainty, calibration curves were generated using maximum uncertainties in each calibration voltage point. This led to an uncertainty range in liquid velocity and turbulence intensity which is shown as error bars in figure 4. Note that the error bars encompass the scatter in the repeated data points. Note also that the error bars represent calibration bias uncertainty; the relative difference in velocity and turbulence intensity between the test cases would always be present. This is because the HFA measurements for the test cases were taken in quick succession at each specified Y location, before moving to the next Y location.

The liquid velocity obtained via calibrated HFA measurements can be compared with the interfacial velocity obtained by cross-correlation in figure 4. Most of the data points below Y/t=0.06 agree within ±10 %. This indicates that, near the wall, the interfaces in the film move at a mean velocity which is close to that of the liquid phase. Beyond Y/t=0.05, the interfacial velocity begins to rise more steeply. This seems to be a logical result as the high velocity gas core must begin to influence the velocity of the liquid waves near the outer region of the film. However, the liquid velocity, especially for Cases 2 and 3, do not show this trend. It is likely that the calibration

REPRODUCED AT GOVT EXPENSE # 49

for liquid velocity becomes inaccurate as the void fraction increases beyond a certain point. For Cases 2 and 3, near *Y/t*=0.06, the void fraction exceeds 0.65, and the liquid phase is probably in the form of waves and droplets. These waves and droplets strike the probe and, as a result, may produce biased velocity fields. For void fractions under 0.5, the liquid field is largely continuous, and the calibration is more accurately applied.

The measured liquid turbulence intensities show a peaking near the wall and a relatively constant profile throughout the rest of the film. These observations are consistent with those of Lorencez, *et al.* (1997) who studied horizontal gas-liquid stratified flow. Their study also showed that the liquid turbulence level increased in the presence of a shearing gas flow. Here, the near wall turbulence level for Case 1 is greater than that for Cases 2 and 3, and all are higher than for single-phase liquid flow. The measured total pressure gradient is significantly higher for Case 1 and, since the mean velocity near the wall is about the same as Case 2, would seem to be related to the turbulence level in the film. This relationship is examined in more detail in the following section.

3.2.3 Law-of-the-Wall Formulation for Wall Shear

An expression for wall shear as a function of fluid viscosity, fluid velocity and turbulent energy may be derived using single-phase law-of-the-wall for smooth walls as:

$$u^+ = \frac{1}{\kappa}\ln y^+ + C \tag{1}$$

where

$$u^+ = \frac{u}{u_*} \tag{2}$$

$$u_* = \sqrt{\frac{\tau_w}{\rho}} \tag{3}$$

$$y^+ = \frac{y u_*}{\upsilon} \tag{4}$$

Defining $\ln C_2 = \kappa C$, (5)

$$\frac{u}{u_*} = \frac{1}{\kappa}\ln\left(\frac{y u_* C_2}{\upsilon}\right) \tag{6}$$

or

$$\rho\frac{u}{\tau_w} = \frac{1}{u_*}\frac{1}{\kappa}\ln\left(\frac{y u_* C_2}{\upsilon}\right) \tag{7}$$

REPRODUCED AT GOV'T EXPENSE # 49

To relate local shear stress to turbulent kinetic energy, the following assumption is made:

$$\tau_p = \sqrt{C_\mu}\rho k \tag{8}$$

This is a good assumption in equilibrium boundary layers, with no strong accelerations or decelerations, and where the boundary layer is attached ($C_\mu = 0.09$). The quantity τ_p represents the shear stress at a point in the turbulent near wall regime ($y^+ \sim 14$). If $\tau_w \sim \tau_p$, then Eq (7) becomes:

$$\tau_w = \frac{\rho u \sqrt{k}}{\frac{1}{\kappa C_\mu^{0.25}} \ln\left(C_2 C_\mu^{0.25} \frac{\sqrt{k}y}{\upsilon}\right)} \tag{9}$$

where, for single-phase flow over smooth walls:

$\kappa = 0.4$
$C_2 = 7.39$

The data was plotted using wall coordinates in figure 5a. The friction velocity, u_*, was determined from the measured frictional pressure drop as:

$$u_* = \sqrt{\frac{\tau_w}{\rho}} = \sqrt{\frac{1}{\rho}\frac{\Delta P_f}{4}\frac{D_H}{L}} \tag{10}$$

The single-phase liquid profile in figure 5a is in good agreement with the single-phase wall-bounded flow theory, which includes both the viscous sublayer ($y^+ < 14$) and logarithmic zone ($14 < y^+ < 300$). The liquid phase velocity profile for Cases 2 and 3 also agrees reasonably well with the single-phase theory. The liquid phase velocity profile for Case 1, however, does not agree with single-phase theory; although the slope ($1/\kappa$) is nearly the same, the intercept (C) is less. This implies that the film structure is affecting the wall shear and, in fact, is increasing it for a given velocity profile in the film.

Similar trends have been observed in recent studies of wall-bounded bubbly flows. Both Velidandla, *et al.* (1996) and Marie, *et al.* (1997) observed that the slope and intercept of the liquid velocity profile in the logarithmic zone in bubbly flow were lower than in single-phase flow. This is attributed to the increased turbulence level, or effective roughness, near the wall due to the presence of the bubbles. In air-water annular flows, Hewitt, *et al.* (1990) observed that air bubbles were continuously entrained, broken up and released by the rolling action in the liquid film. Because the liquid film in Case 1 is thicker than in Cases 2 and 3, it is likely that roll waves create more bubbles in Case 1, and would therefore help to explain the deviation of the velocity profile from single-phase theory. In figures 6 and 7, still photographs of each annular flow condi-

REPRODUCED AT GOVT EXPENSE # 49

tion reveal that, indeed, more bubbles appear to be present in the liquid film for Case 1 vs. Case 2.

The near wall turbulence levels for Case 1-3 have already been presented; now, Eqs (9) and (10) are used to predict the pressure gradient as a function of turbulent kinetic energy[1], fluid properties, fluid velocity and law-of-the-wall constants. Figure 5b shows the predictions of frictional pressure gradient calculated from the local HFA measurements as well as the direct measurements. The calculated single-phase and Cases 2 and 3 results, using law-of-the-wall constants from single-phase theory, are in reasonable agreement with the direct measurements. On the other hand, the calculated results for Case 1, using law-of-the-wall constants from single-phase theory, are lower than the direct measurements. The comparison improves if modified values of κ and C ($\kappa = 0.43$, $C = 1.2$) are used in Eq (9), as derived from the curve fit in figure 5a for Case 1. It therefore appears that Eq (9) captures the appropriate relationship between turbulence and wall shear in annular flows provided that the proper law-of-the-wall constants are used in the formulation. These constants appear to be equal to the single-phase values in a "clean" annular flow, where the film is thin and where less bubbles are present. If the film is thicker and more turbulent, with bubbles present, the constants, most notably the intercept, C, will decrease. Further experiments over a wider range of annular flow conditions would be necessary to determine the functional relationship between the law-of-the-wall constants and other pertinent flow parameters.

References

Hewitt, G.F., Jayanti, S., and Hope, C.B. (1990) Structure of Thin Liquid Films in Gas-Liquid Horizontal Flow. *Int. J. Multiphase Flow*, **16,** 951-957.

Hewitt, G.F. and Roberts, D.N. (1969) Studies of Two-Phase Patterns by Simultaneous X-Ray and Flash Photography, AERE-M 2159. H.M.S.O.

Hewitt, G.F., and Whalley, P.B. (1989) Chapter 2, Vertical Annular Two-Phase Flow, Multiphase Science and Technology, **4,** Hemisphere Publishing Corp., New York.

Laufer, J. (1951) Investigation of Turbulent Flow in a Two-Dimensional Channel, NACA Rep. 1053.

Lee, S.J. (1982) The Development of a Digital Data Processing System for Two-Phase Turbulence Data, Masters Thesis, Rensselaer Polytechnic Institute, Troy, N.Y.

Lorencez, C., Nasr-Esfahany, M., Kawaji, M., and Ojha, M. (1997) Liquid Turbulence Structure at a Sheared and Wavy Gas-Liquid Interface, *Int. J. Multiphase Flow*, **23,** 205-226.

Marie, J.L., Moursali, E., and Tran-Cong, S. (1997) Similarity Law and Turbulence Intensity Profiles in a Bubbly Boundary Layer at Low Void Fractions, *Int. J. Multiphase Flow*, **23,** 227-247.

[1]The kinetic energy is approximated by $k \sim (u'^2/2)$, where the HFA measurement of u' includes both streamwise and normal fluctuations.

REPRODUCED AT GOVT EXPENSE # 49

Velidandla, V., Putta, S., and Roy, R.P. (1996) Velocity Field in Isothermal Turbulent Bubbly Gas-Liquid Flow Through a Pipe", *Exp. in Fluids*, **21,** 347-356.

Acknowledgements: The author is grateful to SM Ettorre for inspiring this work, to R Kumar for his informative discussions and to C Zarnofsky for his technical assistance.

REPRODUCED AT GOV'T EXPENSE # 49

Table 1: Effect of Threshold Parameters on Calculated Results

j_l (m/s)	j_g (m/s)	*Y/t*	Level (V)	Slope (mV/ms)	α	*U* (m/s)	*u'* (m/s)
1.3	12.8	.012	0.3	.5	.016	2.39	.95
1.3	12.8	.012	0.2	.4	.014	2.37	.96
1.3	12.8	.012	0.2	.5	.009	2.37	.96
1.3	12.8	.012	0.2	.6	.008	2.37	.97
1.3	12.8	.012	0.1	.5	.008	2.36	.97
1.3	12.8	.068	0.3	.5	.50	3.13	.77
1.3	12.8	.068	0.2	.4	.53	3.11	.77
1.3	12.8	.068	0.2	.5	.49	3.13	.78
1.3	12.8	.068	0.2	.6	.48	3.13	.78
1.3	12.8	.068	0.1	.5	.49	3.12	.79
0.65	20.4	.012	0.3	.5	.021	2.52	.78
0.65	20.4	.012	0.2	.4	.024	2.52	.79
0.65	20.4	.012	0.2	.5	.02	2.51	.79
0.65	20.4	.012	0.2	.6	.017	2.51	.79
0.65	20.4	.012	0.1	.5	.019	2.51	.79
0.65	20.4	.068	0.3	.5	.66	3.54	.62
0.65	20.4	.068	0.2	.4	.67	3.54	.63
0.65	20.4	.068	0.2	.5	.66	3.53	.65
0.65	20.4	.068	0.2	.6	.65	3.52	.65
0.65	20.4	.068	0.1	.5	.65	3.52	.66

The shaded areas indicate the threshold parameters and calculated results used in this paper.

REPRODUCED AT GOV'T EXPENSE # 49

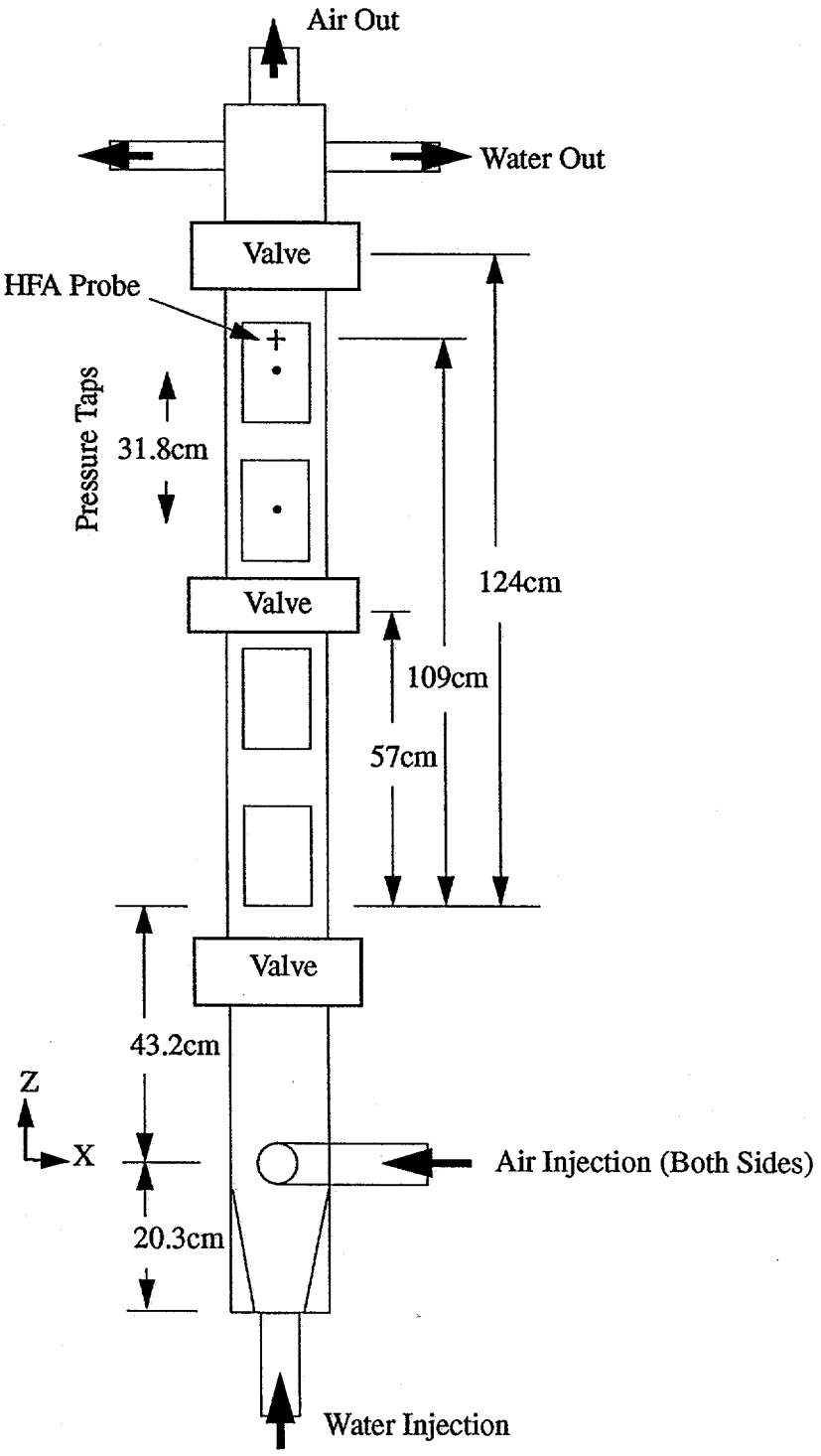

Figure 1. Test Section Schematic

REPRODUCED AT GOVT EXPENSE # 49

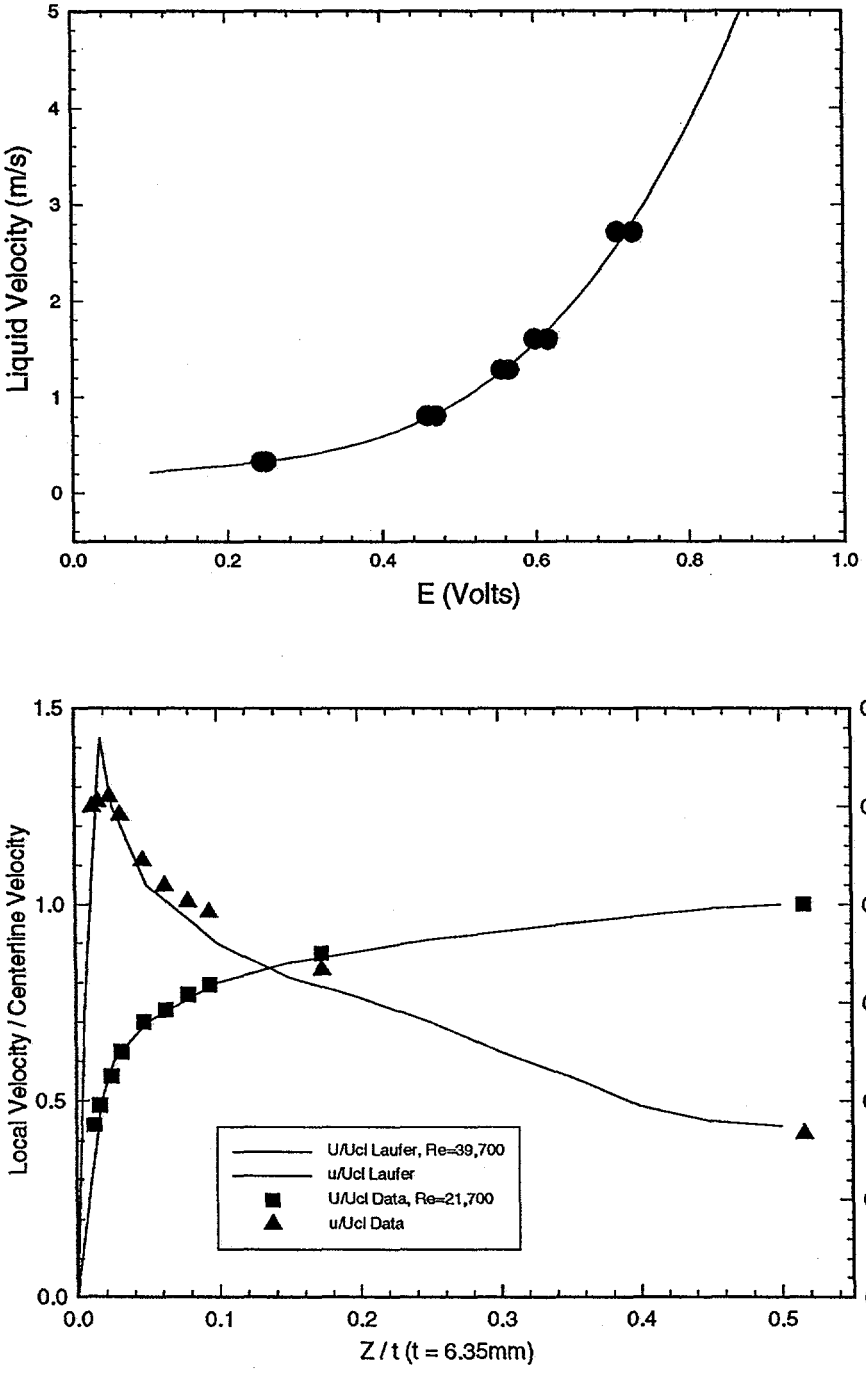

Figure 2. (a) HFA calibration in singe-phase liquid flow (b) Single-phase turbulent profiles compared with Laufer's (1951) data

REPRODUCED AT GOV'T EXPENSE # 49

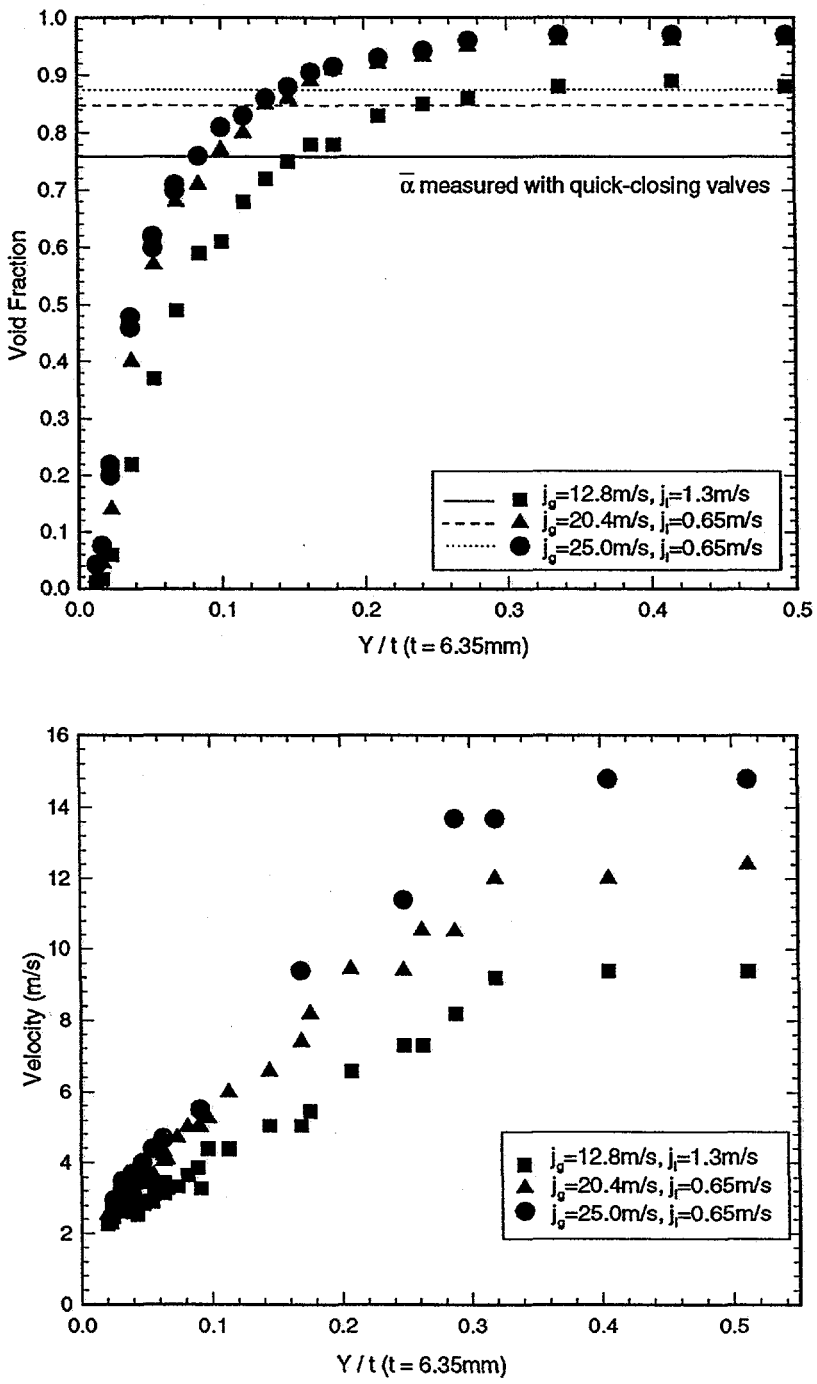

Figure 3. (a) Local HFA void fraction measurements compared to average measurements
(b) HFA interfacial velocity measured using cross-correlation

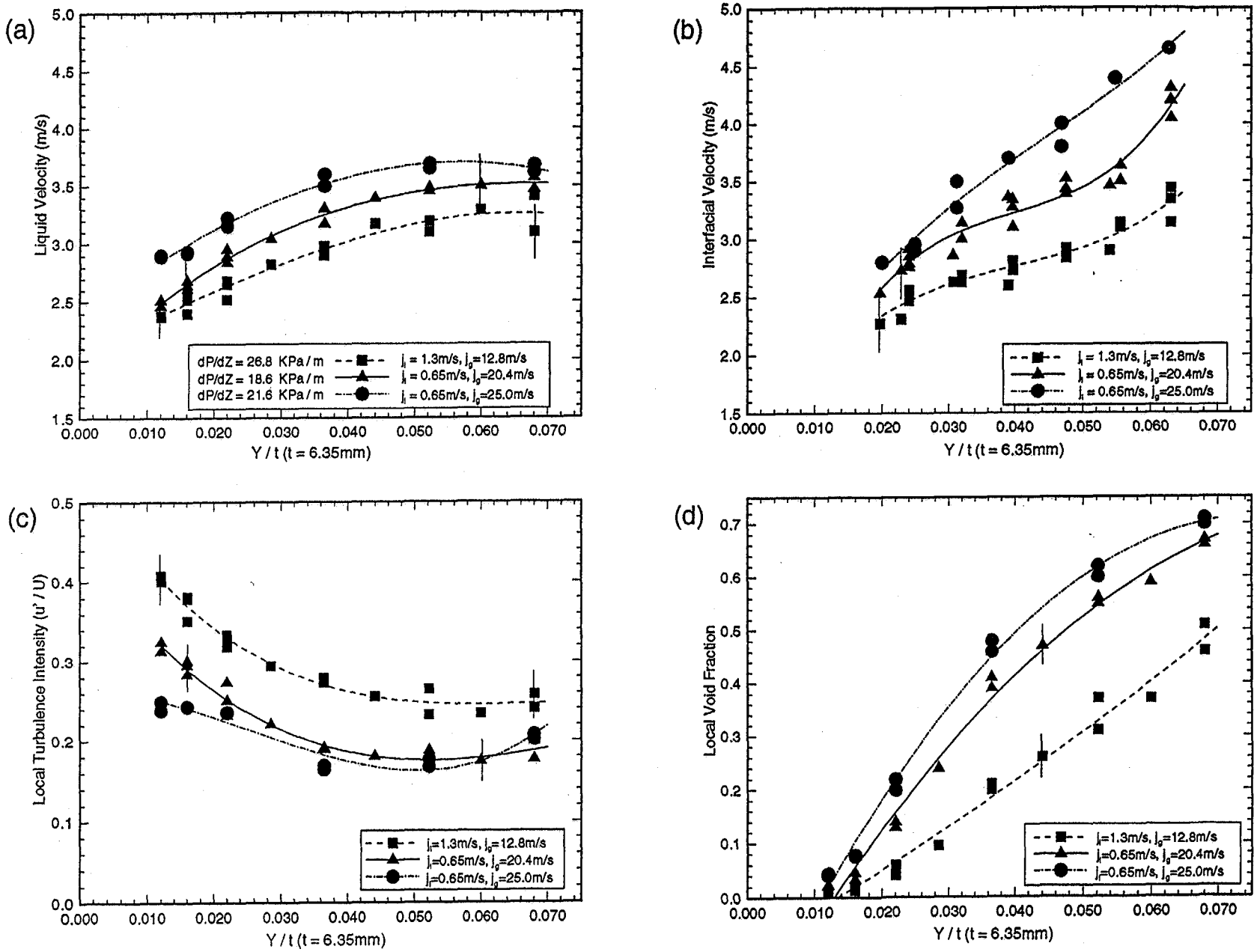

Figure 4. Near-wall HFA data. (a) liquid velocity using calibration (b) interfacial velocity using cross-correlation (c) turbulence intensity (d) void fraction

REPRODUCED AT GOVT EXPENSE # 49
REPRODUCED AT GOVT EXPENSE # 15

REPRODUCED AT GOV'T EXPENSE #.49

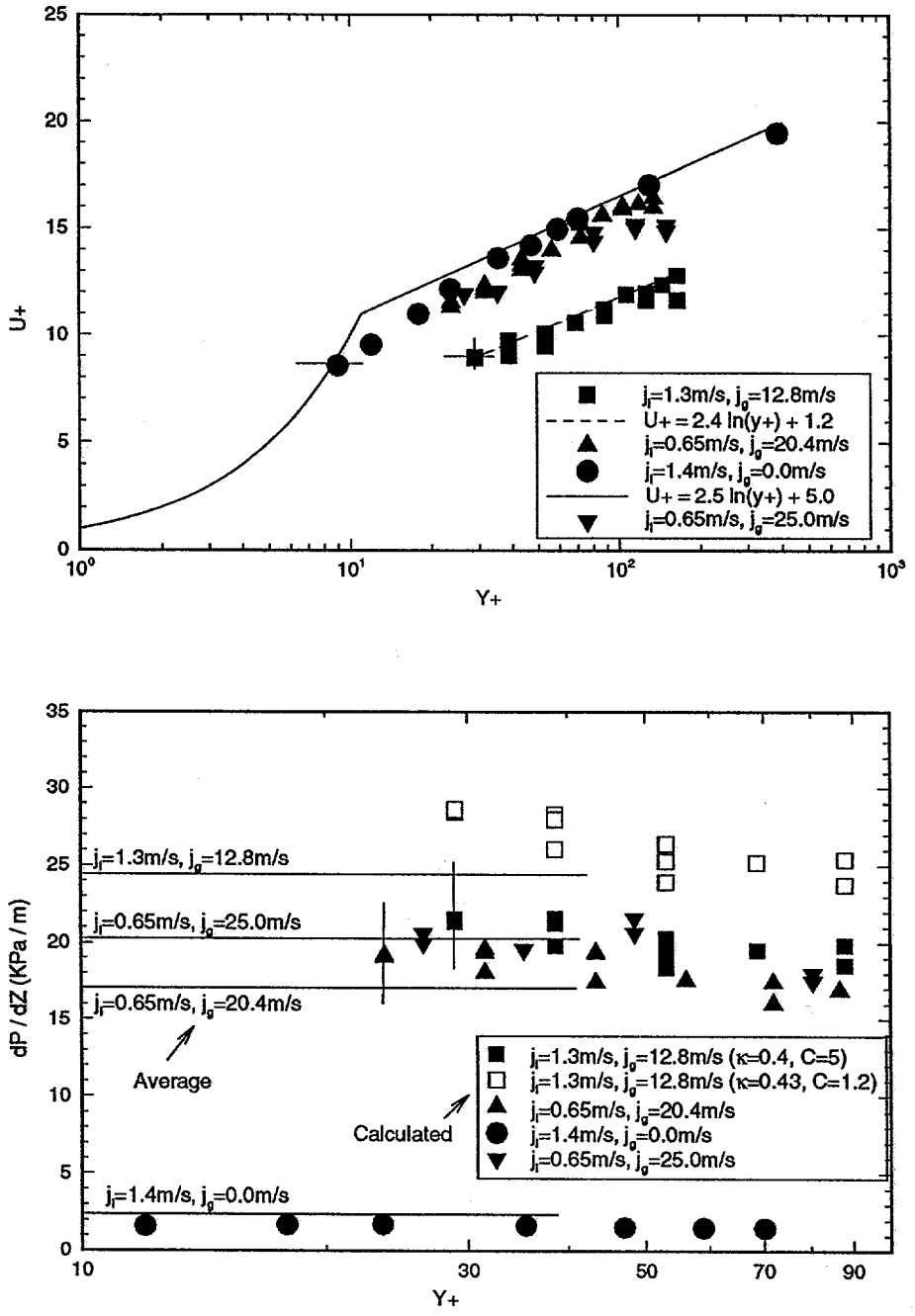

Figure 5. (a) Liquid phase velocity profiles plotted using inner variables
(b) Calculated local frictional dP/dZ from HFA measurements using law-of-wall formaulation compared to average dP/dZ measurements

REPRODUCED AT GOV'T EXPENSE # 49

REPRODUCED AT GOV'T EXPENSE # 15

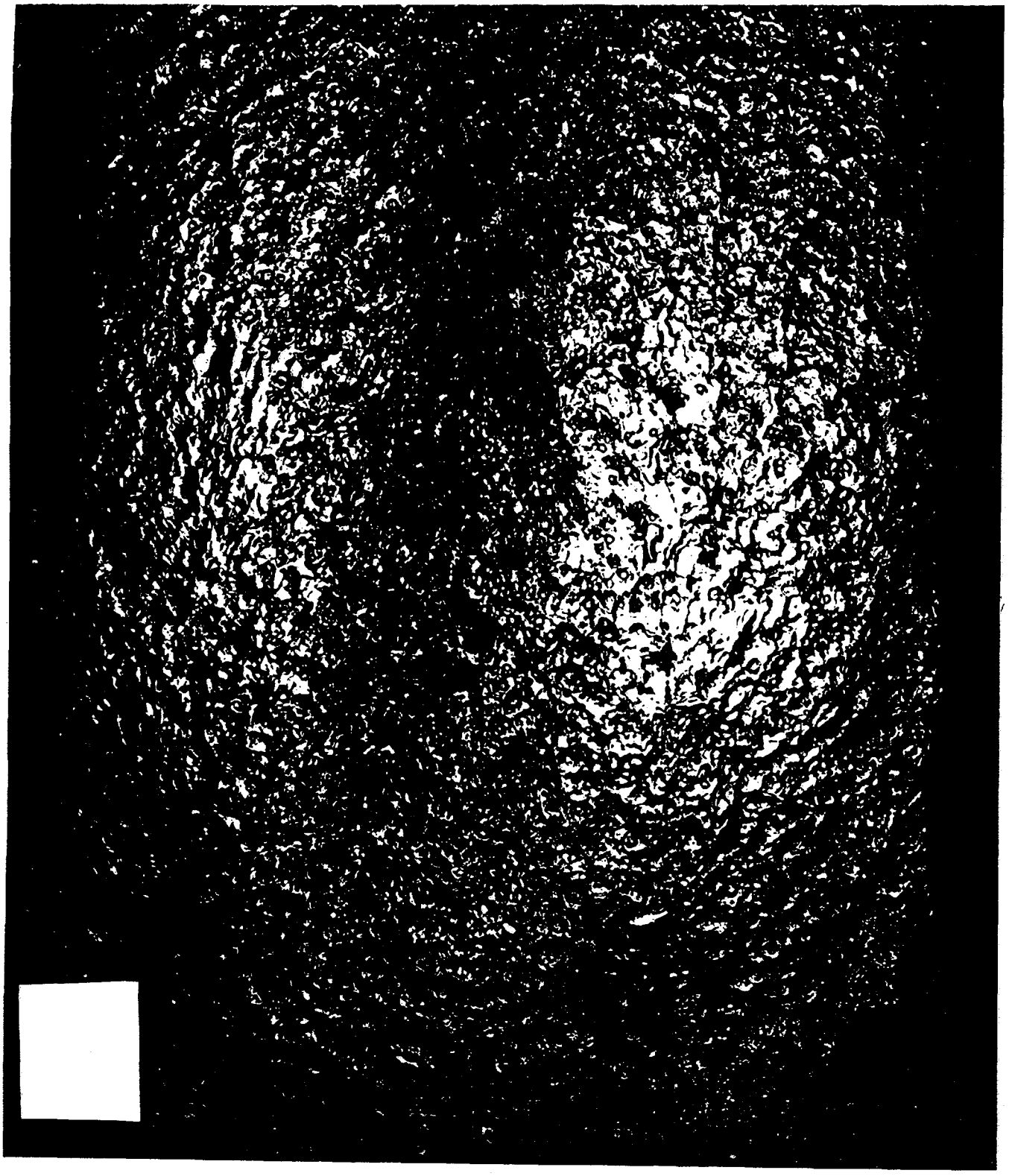

Figure 6. Photograph of Case 1 condition (j_l=1.3m/s, j_g=12.8m/s). Magnification = 2.5.

REPRODUCED AT GOV'T EXPENSE # 49

REPRODUCED AT GOV'T EXPENSE # 15

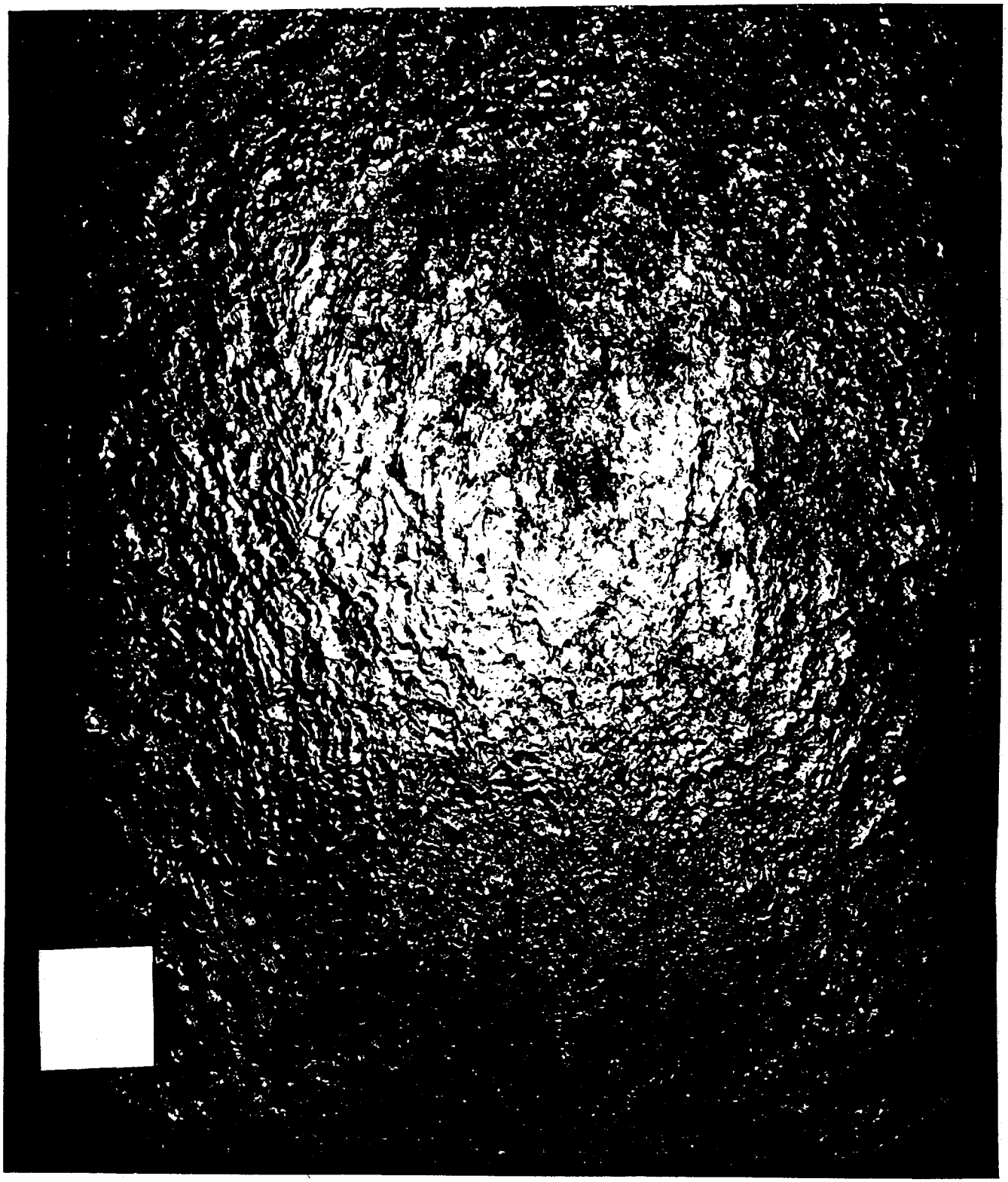

Figure 7. Photograph of Case 2 condition (j_l=0.65m/s, j_g=20.4m/s). Magnification = 2.5.